


RESEARCH

Open Access



The mutational and phenotypic spectrum of *TUBA1A*-associated tubulinopathy

Moritz Hebebrand¹, Ulrike Hüffmeier¹, Regina Trollmann², Ute Hehr³, Steffen Uebe¹, Arif B. Ekici¹, Cornelia Kraus¹, Mandy Krumbiegel¹, André Reis¹, Christian T. Thiel^{1*}  and Bernt Popp^{1†}

Abstract

Background: The *TUBA1A*-associated tubulinopathy is clinically heterogeneous with brain malformations, microcephaly, developmental delay and epilepsy being the main clinical features. It is an autosomal dominant disorder mostly caused by de novo variants in *TUBA1A*.

Results: In three individuals with developmental delay we identified heterozygous de novo missense variants in *TUBA1A* using exome sequencing. While the c.1307G > A, p.(Gly436Asp) variant was novel, the two variants c.518C > T, p.(Pro173Leu) and c.641G > A, p.(Arg214His) were previously described. We compared the variable phenotype observed in these individuals with a carefully conducted review of the current literature and identified 166 individuals, 146 born and 20 fetuses with a *TUBA1A* variant. In 107 cases with available clinical information we standardized the reported phenotypes according to the Human Phenotype Ontology. The most commonly reported features were developmental delay (98%), anomalies of the corpus callosum (96%), microcephaly (76%) and lissencephaly (agyria-pachygyria) (70%), although reporting was incomplete in the different studies. We identified a total of 121 specific variants, including 15 recurrent ones. Missense variants cluster in the C-terminal region around the most commonly affected amino acid position Arg402 (13.3%). In a three-dimensional protein model, 38.6% of all disease-causing variants including those in the C-terminal region are predicted to affect the binding of microtubule-associated proteins or motor proteins. Genotype-phenotype analysis for recurrent variants showed an overrepresentation of certain clinical features. However, individuals with these variants are often reported in the same publication.

Conclusions: With 166 individuals, we present the most comprehensive phenotypic and genotypic standardized synopsis for clinical interpretation of *TUBA1A* variants. Despite this considerable number, a detailed genotype-phenotype characterization is limited by large inter-study variability in reporting.

Keywords: *TUBA1A*, Tubulin, Tubulinopathy, Lissencephaly, Brain malformation, Microcephaly, Developmental delay, Human phenotype ontology

Introduction

The superfamily of tubulin genes is composed of alpha-, beta-, gamma-, delta- and epsilon families. The alpha and beta families, consisting of at least 15 alpha and 21 beta-tubulin genes, respectively [1], encode tubulin proteins which form heterodimers as fundamental components of microtubules [2]. Along with microtubule associated proteins (MAPs) and motor proteins on the

external surface, tubulin proteins participate in substantial cellular processes of intracellular transport, cell division and neuronal migration [3, 4].

In recent years, an increasing number of tubulin genes were linked to a clinically heterogeneous group of disorders, the “tubulinopathies” (*TUBA1A*, MIM#602529; *TUBA8*, MIM#605742; *TUBB2A*, MIM#615101; *TUBB2B*, MIM#612850; *TUBB3*, MIM#602661; *TUBB*, MIM#191130; *TUBG1*, MIM#191135) [5–11]. Tubulinopathies are characterized by a broad spectrum of cortical and sub-cortical malformations and a variety of clinical features. Major cortical anomalies include lissencephaly (agyria-pachygyria), polymicrogyria or polymicrogyria-like cortical

* Correspondence: Christian.Thiel@uk-erlangen.de

†Christian T. Thiel and Bernt Popp contributed equally to this work

¹Institute of Human Genetics, Friedrich-Alexander-Universität Erlangen-Nürnberg (FAU), Schwabachanlage 10, 91054 Erlangen, Germany
Full list of author information is available at the end of the article



dysplasia and cortical gyral simplification. Subcortical anomalies affect the corpus callosum, the cerebellar vermis, the brainstem, the basal ganglia and the cerebellum. Further clinical features are microcephaly, global developmental delay and epilepsy [12, 13]. To date, *TUBA1A* represents the main tubulinopathy gene and accounts for 4–5% of all lissencephaly cases [14, 15].

Using exome analysis in three unrelated individuals with severe developmental delay we identified three heterozygous de novo missense variants in the *TUBA1A* gene. We extensively reviewed and systematically reanalyzed available public data to provide a standardized synopsis of described variants together with reported neuroradiological and clinical features of *TUBA1A*-associated tubulinopathy. We used this comprehensive information to perform a detailed analysis of the genotypic and phenotypic spectrum highlighting a possible genotype-phenotype relationship and probable bias in reporting.

Materials and methods

Clinical reports of 3 novel cases

For the purpose of this study the clinical course of three individuals, who presented between 1999 and 2016 at our Center of Developmental Neurology and Social Pediatrics for investigation of the etiology of developmental delay, was retrospectively summarized after pathogenic missense variants in *TUBA1A* had been identified. In summary, we present novel clinical data for two boys aged 13 years 7 months (individual i084n) and 11 years 6 months (individual i085n) and a 9 years 3 months old girl (individual i086n) with global developmental delay and neuroradiological abnormalities due to *TUBA1A*-associated tubulinopathy. The identification of the *TUBA1A* variant in the girl was part of a previous publication without detailed clinical description (reported as ID S_006) [16]. Narrative case reports with representative MRI planes for all three individuals and facial phenotype pictures for i086n (Additional file 1: Figure S1-S3) are provided in the Supplementary notes.

Exome sequencing

Informed written consent was obtained for all participants. The study was approved by the Ethical Committee of the Medical Faculty of the Friedrich-Alexander-Universität Erlangen-Nürnberg. DNA from peripheral blood lymphocytes was extracted using standard methods. Exome sequencing was performed after SureSelect v5 (i085n, i086n) and v6 (i084n) targeted capturing on HiSeq 2500 for i084n and i085n (Trio analysis [17]) and i086n (Exome Pool-Seq [16]). After mapping of sequence reads to the GRCh37/hg19 reference genome and variant calling using standard methods for the trio analysis [17] or as described by Popp et al. for the exome Pool-Seq [16], variants in coding regions including splice sites were selected based on

population frequency (gnomAD) and computational prediction scores, e.g. CADD score [18]. Variants were confirmed, and segregation tested by Sanger sequencing.

Review of reported *TUBA1A* cases from literature and databases

We identified 112 articles, published between 01/2007 and 06/2018, from PubMed applying the search term “*TUBA1A*”. Of these, 28 provided clinical reports and were thus included in this study. All available clinical data was standardized in accordance to terms of the Human Phenotype Ontology (HPO) [19]. In contrast to a previously established classification combining cortical and subcortical features like “classic lissencephaly”, “lissencephaly with cerebellar hypoplasia”, “lissencephaly with agenesis of the corpus callosum” and “centrally predominant pachygyria” [12, 20], we analyzed the features independently. If only the classification was mentioned, we used the independent underlying features where HPO terms were available (e.g. “micro-lissencephaly”: microcephaly HP:0000252 + agyria HP:0031882). Nevertheless, we kept composite terms typically used together in the literature such as “agyria-pachygyria” (HP:0031882, HP:0001302) if they affected the same brain structure. Data assessment comprised 11 neuroradiological features, including anomalies of cortical gyration, corpus callosum, brainstem, basal ganglia, internal capsule, cerebellum, cerebellar vermis, hippocampus, ventricular dilatation, 4th ventricle dilatation, grey matter heterotopia, and other radiological findings. Clinical features included congenital microcephaly, microcephaly, developmental delay, epilepsy, neuro-ophthalmological findings including strabismus and nystagmus, other neurological symptoms including spasticity and muscular hypotonia, and additional features (HPO terms shown in Tables 1 and 2, Additional file 2).

We further included available likely pathogenic or pathogenic variants from ClinVar [21], denovo-db [22] and DECIPHER [23]. As phenotype information was insufficient in most of these database cases, only variant information was included.

All variants were harmonized to the NM_006009.3 transcript of the GRCh37/hg19 human reference genome based on Human Genome Variation Society (HGVS) recommendations using the Mutalyzer [24] web services. To ensure consistency in the clinical interpretation we independently applied the American College of Medical Genetics and Genomics (ACMG) criteria [25] to all variants with the WGLAB InterVar-tool [26].

Protein structure analysis of the tubulin alpha-1A variants

Using R and ggplot2 [27] we analyzed spatial distribution of all variants in the linear gene model to provide an insight into the variant distribution. Utilizing Pymol

Table 1 Neuroradiological features of *TUBA1A*-associated tubulinopathy

Clinical information	Born n (%)	Fetuses n (%)	Total n (%)
Number of reported cases	87 (100.0)	20 (100.0)	107 (100.0)
Sex	34f/38 m/15 ns	7f/12 m/1 ns	41f/50 m/16 ns
Abnormality of the Corpus Callosum (HP:0001273)	82/86 (95.3)	20/20 (100.0)	102/106 (96.2)
Agenesis (HP:0001274)	16/86 (18.6)	16/20 (80.0)	32/106 (30.2)
Partial agenesis (HP:0001338)	14/86 (16.3)	1/20 (5.0)	15/106 (14.2)
Dysplastic (HP:0006989)	14/86 (16.3)	3/20 (15.0)	17/106 (16.0)
Hypoplasia (HP:0002079)	33/86 (38.4)	0/20 (0.0)	33/106 (31.1)
Partial agenesis, hypoplastic (HP:0001338, HP:0002079)	5/86 (5.8)	0/20 (0.0)	5/106 (4.7)
Normal	4/86 (4.7)	0/20 (0.0)	4/106 (4.7)
No information available	1/87 (1.2)	0/20 (0.0)	1/107 (0.9)
Abnormal cortical gyration (HP:0002536)	76/77 (98.7)	19/19 (100.0)	95/96 (99.0)
Lissencephaly (HP:0006818)	50/77 (64.9)	17/19 (89.5)	67/96 (70.0)
Agyria (HP:0031882)	12/77 (15.6)	15/19 (78.9)	27/96 (28.1)
Agyria-pachygyria (HP:0031882, HP:0001302)	15/77 (19.5)	1/19 (5.3)	16/96 (16.7)
Pachygyria (HP:0001302)	23/77 (29.9)	1/19 (5.3)	24/96 (25.0)
Polymicrogyria (HP:0002126)	16/77 (20.8)	2/19 (10.5)	18/96 (18.8)
Perisylvian-polymicrogyria (HP:0012650)	10/77 (13.0)	0/20 (0.0)	10/96 (10.4)
Cortical gyral simplification (HP:0009879)	5/77 (6.5)	0/20 (0.0)	5/96 (5.2)
Unspecific	5/77 (6.5)	0/20 (0.0)	5/96 (5.2)
Normal	1/77 (1.3)	0/20 (0.0)	1/96 (1.0)
No information available	10/87 (11.5)	1/20 (5.0)	11/107 (10.3)
Abnormality of the cerebellar vermis (HP:0002334)	60/64 (93.8)	18/18 (100.0)	78/83 (94.0)
Hypoplasia (HP:0001320)	44/64 (68.8)	12/18 (66.7)	56/83 (67.5)
Dysgenesis (HP:0002195)	16/64 (25.0)	6/18 (33.3)	22/83 (26.5)
Normal	5/64 (7.8)	0/20 (0.0)	5/83 (6.0)
No information available	22/87 (25.3)	2/20 (10.0)	24/107 (22.4)
Abnormality of the basal ganglia (HP:0002134)	50/50 (100.0)	8/9 (88.9)	58/59 (98.3)
Dysgenesis (HP:0025102)	50/50 (100.0)	8/9 (88.9)	58/59 (98.3)
Normal	0/50 (0.0)	1/9 (11.1)	1/59 (1.7)
No information available	37/87 (42.5)	11/20 (55.0)	48/107 (44.9)
Abnormality of the brainstem (HP:0002363)	39/47 (83.0)	18/18 (100.0)	57/65 (87.7)
Hypoplasia (HP:0002365)	24/47 (51.1)	8/18 (44.4)	32/65 (49.2)
Pons hypoplasia (HP:0012110)	6/47 (12.8)	10/18 (55.6)	16/65 (24.6)
Dysplasia (HP:0002508)	9/47 (19.1)	0/20 (0.0)	9/65 (13.8)
Normal	8/47 (17.0)	0/20 (0.0)	8/65 (12.3)
No information available	40/87 (46.0)	2/20 (10.0)	42/107 (39.3)
Ventricular dilatation (HP:0002119)	43/43 (100.0)	6/6 (100.0)	49/49 (100.0)
Fourth ventricle dilatation (HP:0002198)	19/43 (44.2)	1/6 (16.7)	20/49 (40.8)
No information available	44/87 (50.6)	14/20 (70.0)	58/107 (54.2)
Abnormality of the cerebellum (HP:0001317)	22/32 (68.8)	16/17 (94.1)	38/49 (77.6)
Dysplasia (HP:0007033)	4/32 (12.5)	6/17 (35.3)	10/49 (20.4)
Hypoplasia (HP:0001321)	16/32 (50.0)	10/17 (58.8)	26/49 (53.1)
Agenesis (HP:0012642)	1/32 (3.1)	0/20 (0.0)	1/49 (2.0)
Normal	10/32 (31.3)	1/17 (5.9)	11/49 (22.4)

Table 1 Neuroradiological features of *TUBA1A*-associated tubulinopathy (Continued)

Clinical information	Born n (%)	Fetuses n (%)	Total n (%)
No information available	55/87 (63.2)	3/20 (15.0)	58/107 (54.2)
Abnormal morphology hippocampus (HP:0025100)	24/29 (82.8)	5/8 (62.5)	30/38 (78.9)
Hypoplasia (HP:0025517)	6/29 (20.7)	3/8 (37.5)	9/38 (23.7)
Dysgenesis (HP:0025101)	18/29 (62.1)	2/8 (25.0)	20/38 (52.6)
Normal	5/29 (17.2)	3/8 (37.5)	8/38 (21.1)
No information available	58/87 (66.7)	12/20 (60.0)	69/107 (64.5)
Abnormality of the internal capsule (HP:0012502)	24/25 (96.0)	1/19 (100.0)	25/26 (96.2)
Anterior limb thinned or absent	13/25 (52.0)	0/20 (0.0)	13/26 (50.0)
Normal	1/25 (4.0)	0/20 (0.0)	1/26 (3.8)
No information available	62/87 (71.3)	19/20 (95.0)	81/107 (75.7)
Grey matter heterotopia (HP:0002281)	11/13 (84.6)	14/15 (93.3)	25/28 (89.3)
Olivary	5/13 (38.5)	6/15 (40.0)	11/28 (39.3)
Absent	2/13 (15.4)	1/15 (6.7)	3/28 (10.7)
No information available	74/87 (85.1)	5/20 (25.0)	79/107 (73.8)
Other radiological features	12/12 (100)	8/8 (100.0)	20/20 (100.0)
Abnormal morphology of the olfactory bulb (HP:0040327)	2/12 (16.7)	6/8 (75.0)	8/20 (40.0)
No information available	75/87 (86.2)	12/20 (60.0)	87/107 (81.3)

F Female, M Male, N Number, N/A Not applicable, NS Not specified

(Version 1.8.6.0; Schrödinger, LLC) installed through Conda (Version 4.4.9 build 3.0.27 with Python 2.7.14; Anaconda Inc.) publicly available tertiary protein structure data of *TUBA1A* (PDB-ID: J5CO [28]) was used to classify variants in different groups of potential functional effects as suggested previously [29]. This classification is based on the interaction of the tubulin monomer with neighboring tubulin proteins within the polymer (heterodimer, protofilament, microtubule), with MAPs, or motor proteins. While functional evidence was present only for a minority of the variants [5, 30], most mutational effects are based on localization-dependent predictions. As a template we used 51 already classified *TUBA1A* variants [31] likely affecting the binding of microtubule associated proteins (“MAP binding”) or motor proteins, the tubulin folding (“Tubulin folding”), heterodimer and microtubule stability (“Intradimer interaction” and “Longitudinal interaction”) the formation of the hollow tubular structure of the microtubule (“Lateral interaction”) [32, 33] or microtubule dynamics, protein folding and heterodimer stability (“GTP [Guanosin triphosphat] binding”) [29, 32]. The specific detrimental effect of variants facing the luminal protein surface (“Lumen facing”) is currently unknown.

Computational analyses of *TUBA1A* missense variant spectrum

We here analyzed the ability of six different computational classifiers (three ensemble scores: CADD, M-CAP, REVEL and the three commonly used scores Polyphen-2, SIFT,

MutationTaster) to discriminate pathogenic and neutral population variants by generating all possible missense variants for *TUBA1A*. First all single base exchanges were generated in the *TUBA1A* gene region of the GRCh37/hg19 reference (chr12[hg19]:49578578–49,583,107) as variant call format (VCF) file. These were then annotated with computational scores and databases from dbNSFP [34] version 2.9.3 and variant frequencies from the gnomAD database [35] version 2.0.1 using SnpEff/SnpSift [36]. Missense variants affecting the NM_006009.3 transcript of *TUBA1A*, excluding variants, which were additionally annotated as potentially affecting splicing, were selected. R language [37] version 3.4.3 with RStudio IDE version 1.1.383 (RStudio, Inc.) with packages from the tidyverse/ggplot2 [27] collection were used for plotting and analysis of this variant data provided in the Additional file 2. To analyze possible mutational hotspots, we generated density plots of pathogenic missense variant frequencies reported in the literature and missense variants reported in controls from gnomAD with the “geom_density” function (“adjust” parameter set to 1/4) in ggplot2. To analyze protein regions of higher conservation we plotted all missense variants sorted by amino-acid position with each respective computational score and fitted generalized additive models using the “geom_smooth” function in ggplot2 to produce a smoothed line. Additionally, variants and scores were plotted as scatter and violin plots and two-sided Wilcoxon signed-rank test from the ggsignif package was used to determine whether there was a statistically significant difference between four different

Table 2 Clinical features of *TUBA1A*-associated tubulinopathy

Clinical information	Born n (%)	Fetuses n (%)	Total n (%)
Number of reported cases	87 (100.0)	20 (100.0)	107 (100.0)
Sex	34f/38 m/15 ns	7f/12 m/1 ns	41f/50 m/16 ns
Microcephaly (HP:0000252)	47/53 (88.7)	10/20 (50.0)	57/75 (76.0)
Normal	8/53 (15.1)	10/20 (50.0)	18/75 (24.0)
No information available	32/87 (36.8)	0/20 (0.0)	32/107 (29.9)
Congenital microcephaly (HP:0011451)	25/36 (69.4)	n/a	25/36 (69.4)
Normal	11/36 (30.6)	n/a	11/36 (30.6)
No information available	51/87 (58.6)	n/a	51/87 (58.6)
Global developmental delay (HP:0001263)	52/53 (98.1)	n/a	52/53 (98.1)
Normal	1/53 (1.9)	n/a	1/87 (1.1)
No information available	34/87 (39.1)	n/a	34/87 (39.1)
Other neurological symptoms	39/40 (97.5)	n/a	38/40 (95.0)
Spasticity (HP:0001257)	19/40 (47.5)	n/a	23/40 (57.5)
Muscular hypotonia (HP:0001252)	10/40 (25.0)	n/a	16/40 (40.0)
Spasticity and muscular hypotonia (HP:0001257, HP:0001252)	6/40 (15.0)	n/a	6/40 (15.0)
Other	4/40 (10.0)	n/a	4/40 (10.0)
Normal	1/40 (2.5)	n/a	1/40 (2.5)
No information available	47/87 (54.0)	n/a	47/87 (54.0)
Epilepsy (HP:0001250)	37/51 (72.5)	n/a	37/52 (71.2)
Generalized tonic-clonic seizures (HP:0002069)	19/51 (37.3)	n/a	19/52 (36.5)
Infantile spasms (HP:0012469)	4/51 (7.8)	n/a	4/52 (7.7)
Generalized tonic-clonic seizures and infantile spasms (HP:0002069, HP:0012469)	5/51 (9.8)	n/a	5/52 (9.6)
Focal seizures (HP:0007359)	8/51 (15.7)	n/a	9/52 (17.3)
Absent	15/51 (29.4)	n/a	15/52 (28.8)
No information available	35/87 (40.2)	n/a	35/87 (40.2)
Neuroophthalmological features	26/29 (89.7)	1/5 (20.0)	27/35 (77.1)
Strabismus (HP:0000486)	14/29 (48.3)	n/a	14/35 (40.0)
Nystagmus (HP:0000639)	3/29 (10.3)	n/a	3/35 (8.6)
Strabismus and nystagmus (HP:0000486, HP:0000639)	4/29 (13.8)	n/a	4/35 (11.4)
Optic nerve hypoplasia (HP:0008058)	6/29 (20.7)	1/5 (20.0)	7/35 (20.0)
Absent	4/29 (13.8)	4/5 (80.0)	8/35 (22.9)
No information available	57/87 (65.5)	15/20 (75.0)	72/107 (67.3)
Facial anomalies (HP:0000271)	21/29 (72.4)	9/15 (60.0)	30/44 (68.2)
Micro-/retrognathia	6/29 (20.7)	7/15 (46.7)	13/44 (30.0)
Absent	8/29 (27.6)	6/15 (40.0)	14/44 (31.8)
No information available	58/87 (66.7)	5/20 (25.0)	63/107 (58.9)

F Female, M Male, N Number, N/A Not applicable, NS Not specified

missense variant groups (“clinical review”, “database”, “gnomAD”, “simulated”). “Clinical review” included variants from individuals with available phenotype information from our literature review and the three cases reported here, “database” included (likely) pathogenic variants from databases like ClinVar without clinical information, “gnomAD” included all variants present in healthy controls without neurodevelopmental disorders from the

gnomAD database, and “simulated” all other possible missense variants in *TUBA1A*.

Analysis of genotype-phenotype relation

We used the curated set of clinical information and corresponding harmonized variant information to analyze a possible genotype-phenotype relationship by comparing the radiological and clinical features with variant characteristics.

We visualized and structured the acquired categorical data into a grid plot using ggplot2 and the tidyverse [27] package for hypothesis formation. Based on this presentation we used the vcd package [38] to analyze the relationship between variant characteristics and clinical data of the individuals by generating mosaic or association plots. As many values in the resulting contingency tables contained values below five, we estimated *p*-values using a two-sided Fisher's exact test with the "simulate.p.value" setting based on 2000 replicates in R. One-letter amino-acid nomenclature is used in the resulting plots because of space constraints.

Results

Results of exome sequencing in 3 affected individuals

We identified three heterozygous missense variants c.518C > T, c.1307G > A, and c.641G > A in *TUBA1A*. Segregation analysis demonstrated that all variants were de novo. The missense variant c.518C > T, p.(Pro173Leu) identified in individual i084n and the missense variant c.641G > A, p.(Arg214His) in individual i086n, located in exon 4 of *TUBA1A*, were both previously reported either in an affected individual with autism spectrum disorder [39] (c.518C > T, p.(Pro173Leu)) or in several affected individuals with developmental delay and complex cerebral malformations [20, 40] (c.641G > A, p.(Arg214His)). The heterozygous missense variant c.1307G > A, p.(Gly436Asp) identified in individual i085n was absent in the unaffected parents (de novo, sample identity confirmed), not listed in gnomAD, located in a highly conserved domain and multiple lines of computational evidence predicted a deleterious effect. Thus, we classified all variants as pathogenic (class 5) in accordance with the ACMG criteria.

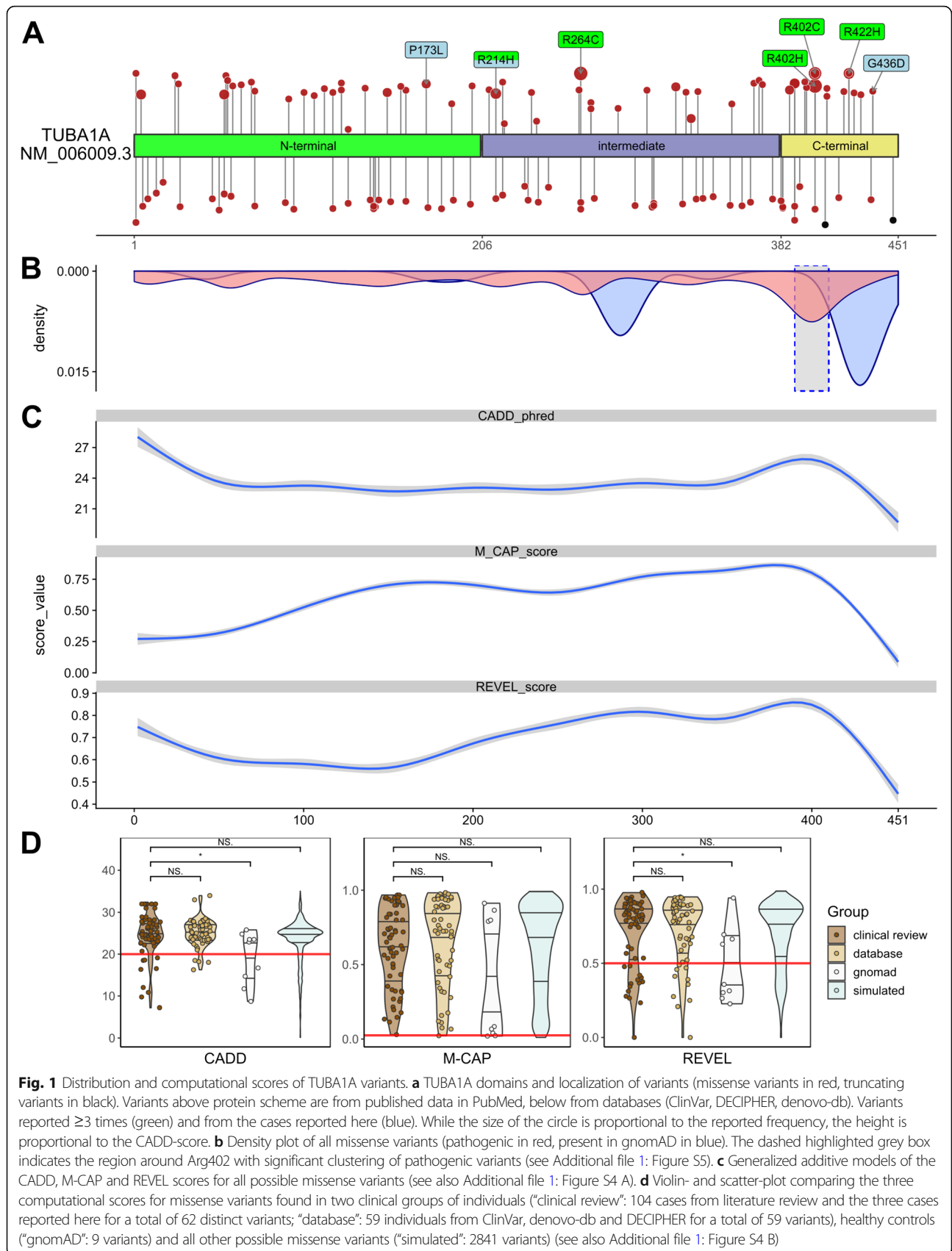
Mutational spectrum and distribution of *TUBA1A* variants

We retrieved a total of 61 distinct variants from 84 born individuals and 20 fetuses from 28 published articles in Pubmed and 59 further distinct variants from databases [5, 13, 15, 20, 30, 39–67]. Moreover we identified one novel variant c.1307G > A, p.(Gly436Asp), not reported in databases or the literature, in one of the three herein described individuals. Of these 121 distinct variants 119 were missense and two led to a premature stop codon located at the C-terminal domain and are predicted to escape nonsense mediated decay. Common recurrent variants were c.1205G > A p.(Arg402His), c.1204C > T p.(Arg402Cys) and c.790C > T p.(Arg264Cys) reported 11, 8 and 10 times, respectively. The Arg402 residue is the most commonly (13.3%) affected amino-acid position (Arg402His, Arg402Cys, Arg402Leu, Arg402Ser). After standardization to the ACMG criteria, 120 of the 121 distinct variants were classified as likely pathogenic or pathogenic (ACMG class 4 or 5) (99.2%) and one variant (c.1224C > A, p.(Tyr408*)) was classified as of unknown significance (VUS, ACMG class 3).

TUBA1A consists of the N-terminal, intermediate and C-terminal domains [68]. Annotation of variants on the linear gene model revealed that variants were distributed all over the *TUBA1A* gene with a statistically significant clustering around the Arg402 residue in exon 4 in the C-terminal domain. This cluster correlates with high computational prediction scores for missense variants (Fig. 1a, b and c; Additional file 1: Figure S4). Variants in the linear C-terminal region predominantly affect the binding of MAPs or motor proteins. Strikingly, computational scores for the different missense variant groups ("clinical review", "database", "gnomAD", "simulated") mostly showed no significant difference (Fig. 1d; Additional file 1: Figure S4). After mapping of the amino acid residues on the 3D protein structure, we observed that most unique variants in "clinical review" (*n* = 121) are predicted to compromise tubulin folding (34.7%) or possibly affecting the interaction with MAPs or motor proteins, such as kinesins and dyneins (24.8%) (Fig. 2). A minority of variants is predicted to affect longitudinal (8.3%), lateral (8.3%) and intradimer (7.4%) interactions, respectively. Finally, 14% of variants are lumen facing and only 2.5% likely affect GTP binding. Considering all assembled variants including the recurrent ones (*n* = 166), the majority (38.6%) is predicted to impair the interaction of MAPs or motor proteins. Of these, 22 affect the Arg402 position. Variants identified in the three individuals i084n, i085n, i086n described here are predicted to affect tubulin folding (c.518C > T, p.(Pro173Leu), MAP binding (c.1307G > A, p.(Gly436Asp) and intradimer interactions (c.641G > A, p.(Arg214His), respectively.

Clinical spectrum of *TUBA1A* variants

Based on available information, major neuroradiological features of *TUBA1A*-associated tubulinopathy include anomalies of the cortical gyration (99.0%, 95/96), with lissencephaly [agyria-pachygyria (HP:0031882, HP:0001302)] and polymicrogyria reported in 70.0% (67/96) and 18.8% (18/96) respectively. Further anomalies affect the basal ganglia (98.3%, 58/59), the corpus callosum (96.2%, 102/106), the capsula interna (96.2%, 25/26) and the cerebellar vermis (94.0%, 78/83). Ventricular dilatation was reported in 100.0% (49/49) and anomalies of the hippocampus in 78.4% (30/38) (Table 1). Clinical features included global developmental delay (98.1%, 52/53), microcephaly (76.0%, 57/75), epilepsy (71.2%, 37/52) and spasticity (62.5%, 25/40) (Table 2). Data missingness ranged from 0.9% (corpus callosum) to 75.7% (internal capsule) for neuroradiological features and from 29.9% (microcephaly) to 67.3% (neuroophthalmological features) for clinical features. We provide a detailed summary of the currently described clinical features in born individuals and fetuses with details of data missingness in Tables 1 and 2.



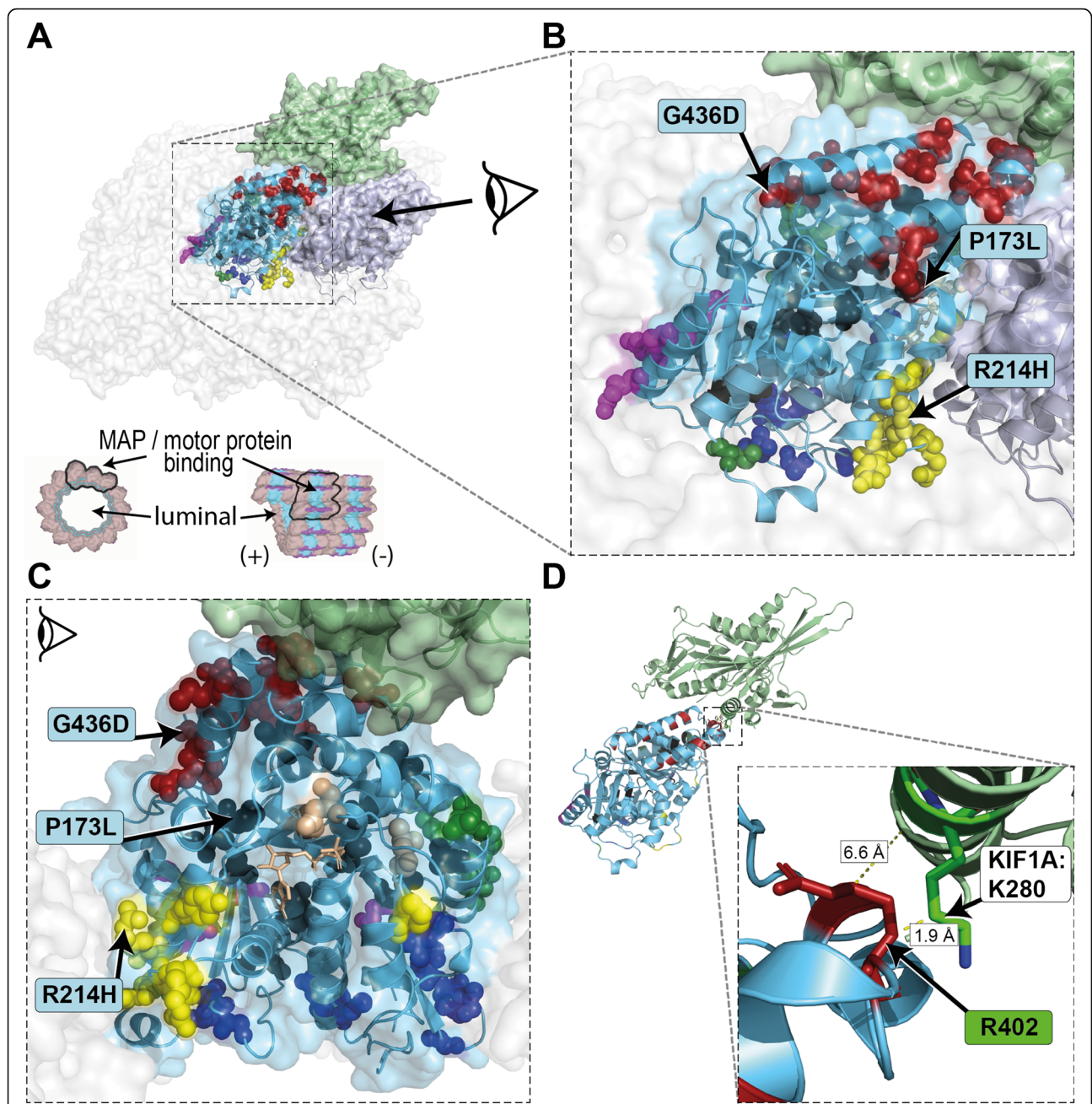


Fig. 2 Mapping of reported variants onto 3D structure of tubulin alpha-1A. **a** TUBA1A (light blue) monomer in the center surrounded by TUBA1A monomers to the lateral sides and TUBB3 monomers to the longitudinal sides (transparent surfaces). The TUBA1A (light blue) - TUBB3 (grey) heterodimer is highlighted and shown in ribbon representation (based on PDB: 5JCO [28]). Exemplary for a motor protein KIF1A (green; PDB: 2HXF [73]) is shown interacting on the external surface. Mutated residues are shown in spheres and likely affect the binding of MAPs or motor proteins (red), tubulin folding (black), intradimer interactions (yellow), longitudinal interactions (magenta), lateral interactions (green) or GTP-binding pocket (beige). Variants on the luminal side are shown in blue. A cross section and longitudinal view of a microtubule [74] is provided for orientation. **b** Close-up view of the central TUBA1A monomer and **c** lateral-view with TUBB3 removed from the dimer. The GTP molecule (beige), required for polymerization, is presented in stick representation. Variants identified in the three individuals i084n (P173L), i085n (G436D), i086n (R214H) described here affect tubulin folding, MAP binding and intradimer interaction, respectively. **d** Simplified representation of TUBA1A and KIF1A with protein surface and spheres removed. The amino acid residue R402 (red stick representation) of TUBA1A is localized near the KIF1A protein, in particular to the amino acid residue K280 (minimal distance 1.9 Å; green stick representation)

Relation between genotype and phenotype

We used the clinical information of the 104 individuals from the “clinical review” group and the herein described three patients (total $n = 107$) to analyze a possible relationship between genotype and phenotype. Individuals with recurrent variants, mostly affecting MAP or motor protein binding, show a similar phenotype combination in the matrix plot (Fig. 3a; see also Additional file 1: Figure S7). Patients with the missense variant p.(Arg402Cys) are mostly described with a cortical-gyration pattern of agyria-pachgyria (“Ag-Pg”), dysplastic corpus callosum (“D”), a cerebellar vermis hypoplasia (“H”) and have no information reported for the brainstem.

Because prenatally diagnosed fetal cases show a more severe phenotype than born individuals, we analyzed a possible contribution of variant characteristics to this observation. The missense variants reported in fetuses and in born individuals showed no significant difference in structural classification (Fig. 3b) and the computational scores did not significantly differ in these two groups (Additional file 1: Figure S6). In addition, the structural groups of missense variants were not overrepresented in females or males and the gender was also not associated with prenatal diagnosis (Fig. 3b).

The visual inspection of the matrix plot (Fig. 3a; Additional file 1: Figure S7) indicated that certain clinical features are enriched in individuals with recurrent variants. Indeed, explorative comparison between missense variants at recurrent and non-recurrent positions confirmed differences in reported clinical features of the individuals carrying these missense variants (Fig. 3c; Additional file 1: Figure S8). Despite our effort to collect all variants and clinical information described for *TUBA1A*-associated tubulinopathy, we did not obtain enough data to further analyze the phenotype differences for these variants.

Finally, we observed that individuals with the same variants and similar phenotypes were often reported together (e.g. Fig. 3a “+” symbol for Arg402Cys reported 5 times in PMID:20466733 [30]). Regarding this observation, we found a significant difference in the use of clinical descriptions in publications describing multiple individuals. Kumar et al. (PMID:20466733 [30]) and Bahi-Buisson et al. (PMID:24860126 [13]) both describe four cases with the de novo missense variant c.1205G > A p.(Arg402His), but Bahi-Buisson et al. more often describes agyria (“Ag”) as cortical gyration pattern. Romaniello et al. (PMID:28677066 [57]) describe perisylvian polymicrogyria (“PsMPG”) as cortical gyration pattern for four (all with different missense variants) of their 14 reported individuals’ variants while this term is only used for 6 other individuals in the entire “clinical review” group (Fig. 3d; Additional file 1: Figure S9).

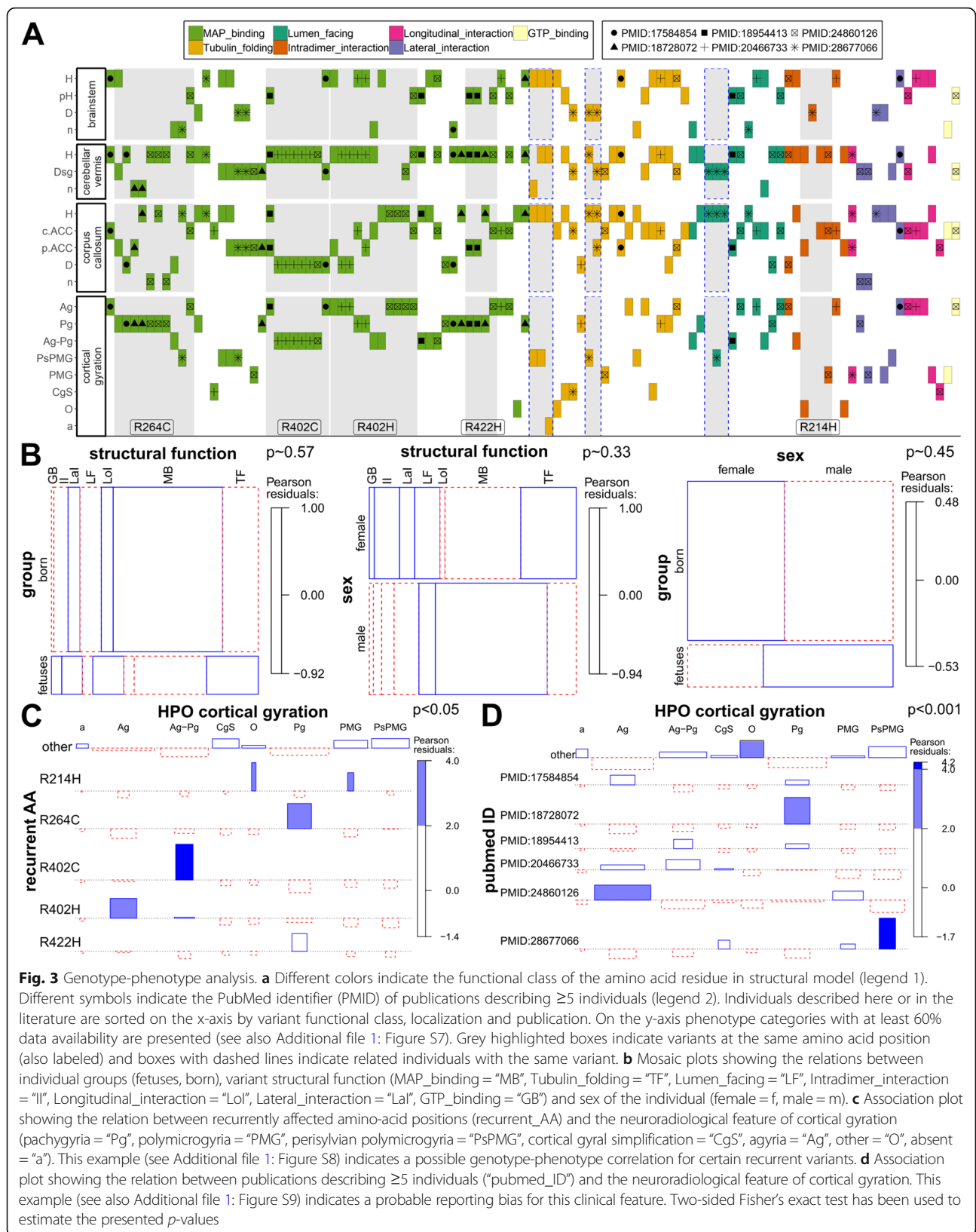
Discussion

In this study, we identified three de novo missense variants in *TUBA1A* in three individuals with global developmental delay and brain malformations. Since the first identification of disease-causing variants in *TUBA1A* in 2007 in two affected individuals with cortical dysgenesis [5], at least 121 distinct heterozygous variants in a total of at least 166 patients including our 3 affected individuals are now described. Our efforts to systematically reanalyze published data enabled insights into the current state of information about *TUBA1A*-associated tubulinopathy.

Anomalies of the corpus callosum ranging from partial to complete agenesis or hypoplasia are with 96.2% (102/106) the predominantly reported feature of *TUBA1A*-associated tubulinopathy. Cortical anomalies are the second leading clinical feature reported in 95/96 individuals (99.0%) followed by dysgenesis of the basal ganglia in 58/59 (98.3%). Two of the herein described individuals (i084n, i085n) also presented these features. Individual i086n had complete agenesis corpus callosum and additionally manifested unilateral optic nerve hypoplasia, a feature linked to *TUBA8*-associated tubulinopathy [6] but also described in individuals with *TUBB2B* [69] and *TUBB3* [9] variants and present in 7/35 (20.0%) of individuals with *TUBA1A*-associated tubulinopathy.

Analysis of the type and localization of all possible 2969 missense variants from the simulation showed that the large majority of *TUBA1A* missense variants are predicted to be deleterious (CADD ≥ 20 : 84.2%, M-CAP $\geq 0,025$: 98.0%, REVEL $\geq 0,5$: 78.8%; Fig. 1d). This is in agreement with an ExAC Z-score [35] of 6.23, confirming that *TUBA1A* is extremely depleted of missense variants in the general population. This resulted in high computational prediction scores independent of causality. Thus, variants might be reported to be likely pathogenic or pathogenic (ACMG class 4 or 5) despite relatively low computational scores and variants found in healthy controls might have scores above the recommended respective thresholds (Fig. 1d). After analyzing the relation of three ensemble computational prediction scores and expected pathogenicity, we concluded that computational prediction scores are of limited utility for predicting pathogenicity in *TUBA1A*. We suggest that segregation with the disease in the family or de novo occurrence, two major criteria of the ACMG guidelines for variant interpretation, are more appropriate for variant classification.

Based on the observation of the mutational distribution we analyzed a possible relationship between genotype and phenotype. We observed clustering of disease-causing variants in the region around the amino acid residue Arg402 (Fig. 1a, b and c, Additional file 1: Figure S2). The residue Arg402 is located in the interaction site of various MAPs or motor proteins [30]



which are involved in different processes including the polymerization and stabilization of microtubules and intracellular vesicle transport [70]. Defects in some MAPs or motor proteins result in a similar clinical spectrum as observed for specific MAP-associated *TUBA1A* variants [30, 71]. Overall, variants of the Arg402 residue and other specific recurrent variants, which are predominantly MAP or motor protein interacting, were previously associated with overlapping neuro-radiological features [13, 30]. Indeed, we could show a non-uniform distribution for reported clinical features and the recurrent variants (Fig. 3c), indicating a possible genotype-phenotype relation. This observation might in part be attributed to detailed structured morphological categorization of brain anomalies used by different authors and individual preferences for certain terms. In addition, difficulties in the interpretation of the radiographic cortical and subcortical anomalies or technical differences in brain imaging could represent a possible confounder. Of note, recurrent variants with similar phenotype combinations were often reported by the same authors indicating a possible observational bias (Fig. 3d), thus limiting the interpretation of these genotype-phenotype relations. Another problem hindering a more detailed investigation is the high degree of missing data we recognized for several phenotypic categories. The directed acyclic graphs structure of HPO allows grouping of specialized terms into less specialized parent terms. Future development of algorithms comparing the phenotypic similarity between groups of individuals with the same or functionally similar pathogenic variants might alleviate some of these problems and allow further characterization of variant specific phenotypes. However, some of these endeavors could be hampered by the difficulty to distinguish between missing information and normal phenotype in published reports. This is especially problematic as HPO describes “phenotype abnormalities” but has no terms for normal phenotypes. We propose standardization in clinical reporting of rare disease cases based on expert recommendations with a minimal scheme covering disease specific phenotypes.

Even though *TUBA1A-associated* tubulinopathy is the most common tubulinopathy form, our results indicate that more clinical and mutational information is necessary to evaluate a potential genotype-phenotype correlation. This became apparent in fetuses, where we and others observed the most severe phenotypic spectrum compared to born cases [13, 20]. This could not be explained by specific properties of the identified variants (Fig. 3b, Additional file 1: Figure S6). We therefore propose that additional variants in other genes or random developmental processes in cellular pathways in the respective individuals are underlying the phenotypic variability. Genome wide and functional studies might

help to allow further characterization into specific clinical groups.

Conclusion

Our systematic reanalysis of published clinical data allowed an explorative investigation of a genotype-phenotype relationship. We found an enrichment of specific radiological features in recurrent variants; however, insufficient data availability, data variability and a possible observer bias were limiting factors for possible associations. A thoroughly conducted clinical examination and the standardized reporting of phenotype and genotype information in online databases, e.g. ClinVar [21] and LOVD [72] are fundamental for the systematic analysis of rare diseases such as *TUBA1A-associated* tubulinopathy.

Additional files

Additional file 1: Figure S1. Cranial MRI planes of individual i084n. **Figure S2.** Cranial MRI planes of individual i085n. **Figure S3.** Cranial MRI planes and clinical pictures of individual i086n. **Figure S4.** Additional computational scores for *TUBA1A* variants. **Figure S5.** Analysis of the variant cluster around amino acid position 400. **Figure S6.** Comparison of computational scores for *TUBA1A* variants identified in fetuses and born individuals. **Figure S7.** Matrix plot of all HPO phenotype categories and all neuroradiological features. **Figure S8.** Association plots for recurrently affected amino-acid positions and all neuroradiological features. **Figure S9.** Association plots publications describing ≥ 5 individuals and all neuroradiological features. **Table S1.** Barthel Index of Activities of Daily Living [3] of the 3 individuals with *TUBA1A* variants. (DOCX 2946 kb)

Additional file 2: Additional information, phenotypes and *TUBA1A* variants. (XLSX 574 kb)

Abbreviations

ACMG: American College of Medical Genetics and Genomics; CMA: Chromosomal microarray; GTP: Guanosintriphosphat; HGVS: Human Genome Variation Society; HPO: Human Phenotype Ontology; MAPs: Microtubule-associated proteins; MRI: Magnetic resonance imaging; OFC: Occipitofrontal circumference; VCF: Variant call format

Acknowledgements

We thank all participants and their families for taking part in this study. We acknowledge the excellent technical support of Angelika Diem, and Heike Friebel-Stange. We also thank the Exome Aggregation Consortium and the groups that provided exome variant data for comparison. A full list of contributing groups can be found at <http://exac.broadinstitute.org/about>. This study utilized data generated by the DECIPHER community. A full list of centers that contributed to data generation is available online from <http://decipher.sanger.ac.uk> and via email from decipher@sanger.ac.uk.

Funding

This study was supported by grants from the German Research Foundation (DFG; grants TH 896/3–4), the Interdisciplinary Centre for Clinical Research (IZKF) of the Friedrich-Alexander-Universität Erlangen-Nürnberg (Project F4) and by the ELAN Fonds (14–08–06-1) of the Faculty of Medicine of the Friedrich-Alexander Universität Erlangen-Nürnberg (FAU) to CT.

Availability of data and materials

All data generated or analysed during this study are included in this published article [and its Additional file 2]. All data is available from the corresponding author on request.

Web resources

gnomAD browser: <http://gnomad.broadinstitute.org/>. Mutalyzer: <https://mutalyzer.nl/>. wInterVar: <http://wintervar.wglab.org/>

Authors' contributions

CT and UH provided all clinical findings and patient samples. MK conducted Array analyses. CK, SU, AE, CT, AR and BP analyzed and interpreted the sequencing data. BP created Figs. 1, 2 and 3 and the supplementary materials. MH performed the literature review and standardization to HPO terms. MH and BP created Fig. 2. BP, MH and CT wrote and edited the manuscript, CK, MK, SU, AE, CT, AR and BP reviewed the draft manuscript. All authors read and approved the final manuscript.

Ethics approval and consent to participate

Informed written consent was obtained for all participants. The study was approved by the Ethical Committee of the Medical Faculty of the Friedrich-Alexander-Universität Erlangen-Nürnberg (180_15Bc).

Consent for publication

Informed written consent for publication was obtained for all participants.

Competing interests

The authors declare that they have no competing interests.

Publisher's Note

Springer Nature remains neutral with regard to jurisdictional claims in published maps and institutional affiliations.

Author details

- ¹Institute of Human Genetics, Friedrich-Alexander-Universität Erlangen-Nürnberg (FAU), Schwabachanlage 10, 91054 Erlangen, Germany.
- ²Department of Pediatrics, Division of Neuropediatrics, Friedrich-Alexander-Universität Erlangen-Nürnberg (FAU), Erlangen, Germany.
- ³Institute of Human Genetics, University of Regensburg, Regensburg, Germany.

Received: 17 October 2018 Accepted: 3 February 2019

Published online: 11 February 2019

References

- Dutcher SK. Long-lost relatives reappear: identification of new members of the tubulin superfamily. *Curr Opin Microbiol.* 2003;6:634–40.
- Hammond JW, Cai D, Verhey KJ. Tubulin modifications and their cellular functions. *Curr Opin Cell Biol.* 2008;20:71–6.
- Kapitein LC, Hoogenraad CC. Building the neuronal microtubule cytoskeleton. *Neuron.* 2015;87:492–506.
- Mandelkow E, Mandelkow EM. Microtubules and microtubule-associated proteins. *Curr Opin Cell Biol.* 1995;7:72–81.
- Keays DA, et al. Mutations in alpha-tubulin cause abnormal neuronal migration in mice and lissencephaly in humans. *Cell.* 2007;128:45–57.
- Abdollahi MR, et al. Mutation of the variant alpha-tubulin TUBA8 results in polymicrogyria with optic nerve hypoplasia. *Am J Hum Genet.* 2009;85:737–44.
- Cushion TD, et al. De novo mutations in the beta-tubulin gene TUBB2A cause simplified gyral patterning and infantile-onset epilepsy. *Am J Hum Genet.* 2014;94:634–41.
- Jaglin XH, et al. Mutations in the beta-tubulin gene TUBB2B result in asymmetrical polymicrogyria. *Nat Genet.* 2009;41:746–52.
- Poirier K, et al. Mutations in the neuronal ss-tubulin subunit TUBB3 result in malformation of cortical development and neuronal migration defects. *Hum Mol Genet.* 2010;19:4462–73.
- Breuss M, et al. Mutations in the beta-tubulin gene TUBB5 cause microcephaly with structural brain abnormalities. *Cell Rep.* 2012;2:1554–62.
- Poirier K, et al. Mutations in TUBG1, DYNC1H1, KIF5C and KIF2A cause malformations of cortical development and microcephaly. *Nat Genet.* 2013;45:639–47.
- Bahi-Buisson N, Cavallin M. Tubulinopathies overview. In: Adam MP, et al, editors. *GeneReviews(R)*. Seattle, Washington; 1993.
- Bahi-Buisson N, et al. The wide spectrum of tubulinopathies: what are the key features for the diagnosis? *Brain.* 2014;137:1676–700.
- Di Donato N, et al. Analysis of 17 genes detects mutations in 81% of 811 patients with lissencephaly. *Genet Med.* 2018;20:1354–64.
- Morris-Rosendahl DJ, et al. Refining the phenotype of alpha-1a tubulin (TUBA1A) mutation in patients with classical lissencephaly. *Clin Genet.* 2008;74:425–33.
- Popp B, et al. Exome Pool-Seq in neurodevelopmental disorders. *Eur J Hum Genet.* 2017;25:1364–76.
- Hauer NN, et al. Clinical relevance of systematic phenotyping and exome sequencing in patients with short stature. *Genet Med.* 2018;20:630–8.
- Kircher M, et al. A general framework for estimating the relative pathogenicity of human genetic variants. *Nat Genet.* 2014;46:310–5.
- Kohler S, et al. The human phenotype ontology in 2017. *Nucleic Acids Res.* 2017;45:D865–76.
- Fallet-Bianco C, et al. Mutations in tubulin genes are frequent causes of various foetal malformations of cortical development including microlissencephaly. *Acta Neuropathol Commun.* 2014;2:69.
- Landrum MJ, et al. ClinVar: improving access to variant interpretations and supporting evidence. *Nucleic Acids Res.* 2018;46:D1062–7.
- Turner TN, et al. denovo-db: a compendium of human de novo variants. *Nucleic Acids Res.* 2017;45:D804–11.
- Firth HV, et al. DECIPHER: database of chromosomal imbalance and phenotype in humans using Ensembl resources. *Am J Hum Genet.* 2009;84:524–33.
- Wildeman M, van Ophuizen E, den Dunnen JT, Taschner PE. Improving sequence variant descriptions in mutation databases and literature using the Mutalyzer sequence variation nomenclature checker. *Hum Mutat.* 2008;29:6–13.
- Richards S, et al. Standards and guidelines for the interpretation of sequence variants: a joint consensus recommendation of the American College of Medical Genetics and Genomics and the Association for Molecular Pathology. *Genet Med.* 2015;17:405–24.
- Li Q, Wang K. InterVar: clinical interpretation of genetic variants by the 2015 ACMG-AMP guidelines. *Am J Hum Genet.* 2017;100:267–80.
- Hadley, W. ggplot2: Elegant graphics for data Analysis, (2016).
- Vemu A, et al. Structure and dynamics of single-isoform recombinant neuronal human tubulin. *J Biol Chem.* 2016;291:12907–15.
- Tischfield MA, Cederquist GY, Gupta ML Jr, Engle EC. Phenotypic spectrum of the tubulin-related disorders and functional implications of disease-causing mutations. *Curr Opin Genet Dev.* 2011;21:286–94.
- Kumar RA, et al. TUBA1A mutations cause wide spectrum lissencephaly (smooth brain) and suggest that multiple neuronal migration pathways converge on alpha tubulins. *Hum Mol Genet.* 2010;19:2817–27.
- Zheng C, Diaz-Cuadros M, Nguyen KCQ, Hall DH, Chalfie M. Distinct effects of tubulin isotype mutations on neurite growth in *Caenorhabditis elegans*. *Mol Biol Cell.* 2017;28:2786–801.
- Nogales E. Structural insight into microtubule function. *Annu Rev Biophys Biomol Struct.* 2001;30:397–420.
- Li H, DeRosier DJ, Nicholson WW, Nogales E, Downing KH. Microtubule structure at 8 Å resolution. *Structure.* 2002;10:1317–28.
- Liu X, Jian X, Boerwinkle E. dbNSFP v2.0: a database of human non-synonymous SNVs and their functional predictions and annotations. *Hum Mutat.* 2013;34:E2393–402.
- Lek M, et al. Analysis of protein-coding genetic variation in 60,706 humans. *Nature.* 2016;536:285–91.
- Cingolani P, et al. A program for annotating and predicting the effects of single nucleotide polymorphisms, SnpEff: SNPs in the genome of *Drosophila melanogaster* strain w1118; iso-2; iso-3. *Fly (Austin).* 2012;6:80–92.
- Team, R.D.C. R: A language and environment for statistical Computing. (2008).
- Meyer, D., Zeileis, A., & Hornik, K. vcd: Visualizing Categorical Data. (2017).
- Iossifov I, et al. The contribution of de novo coding mutations to autism spectrum disorder. *Nature.* 2014;515:216–21.
- Oegema R, et al. Recognizable cerebellar dysplasia associated with mutations in multiple tubulin genes. *Hum Mol Genet.* 2015;24:5313–25.
- Poirier K, et al. Large spectrum of lissencephaly and pachygyria phenotypes resulting from de novo missense mutations in tubulin alpha 1A (TUBA1A). *Hum Mutat.* 2007;28:1055–64.
- Bahi-Buisson N, et al. Refinement of cortical dysgeneses spectrum associated with TUBA1A mutations. *J Med Genet.* 2008;45:647–53.
- Jansen AC, et al. TUBA1A mutations: from isolated lissencephaly to familial polymicrogyria. *Neurology.* 2011;76:988–92.
- Sohal AP, Montgomery T, Mitra D, Ramesh V. TUBA1A mutation-associated lissencephaly: case report and review of the literature. *Pediatr Neurol.* 2012;46:127–31.

45. Mokanzski A, et al. Lissencephaly and band heterotopia: LIS1, TUBA1A, and DCX mutations in Hungary. *J Child Neurol.* 2012;27:1534–40.
46. Cushion TD, et al. Overlapping cortical malformations and mutations in TUBB2B and TUBA1A. *Brain.* 2013;136:536–48.
47. Okumura A, et al. Lissencephaly with marked ventricular dilation, agenesis of corpus callosum, and cerebellar hypoplasia caused by TUBA1A mutation. *Brain and Development.* 2013;35:274–9.
48. Poirier K, et al. Expanding the spectrum of TUBA1A-related cortical dysgenesis to Polymicrogyria. *Eur J Hum Genet.* 2013;21:381–5.
49. Zanni G, et al. Description of a novel TUBA1A mutation in Arg-390 associated with asymmetrical polymicrogyria and mid-hindbrain dysgenesis. *Eur J Paediatr Neurol.* 2013;17:361–5.
50. Hikita N, et al. A case of TUBA1A mutation presenting with lissencephaly and Hirschsprung disease. *Brain and Development.* 2014;36:159–62.
51. Romaniello R, et al. Brain malformations and mutations in alpha- and beta-tubulin genes: a review of the literature and description of two new cases. *Dev Med Child Neurol.* 2014;56:354–60.
52. Kamiya K, Tanaka F, Ikeno M, Okumura A, Aoki S. DTI tractography of lissencephaly caused by TUBA1A mutation. *Neurol Sci.* 2014;35:801–3.
53. Shimojima K, et al. Whole-exome sequencing identifies a de novo TUBA1A mutation in a patient with sporadic malformations of cortical development: a case report. *BMC Res Notes.* 2014;7:465.
54. Yokoi S, et al. TUBA1A mutation can cause a hydranencephaly-like severe form of cortical dysgenesis. *Sci Rep.* 2015;5:15165.
55. Myers KA, Bello-Espinosa LE, Kherani A, Wei XC, Innes AM. TUBA1A mutation associated with eye abnormalities in addition to brain malformation. *Pediatr Neurol.* 2015;53:442–4.
56. Bamba Y, et al. In vitro characterization of neurite extension using induced pluripotent stem cells derived from lissencephaly patients with TUBA1A missense mutations. *Mol Brain.* 2016;9:70.
57. Romaniello R, et al. Tubulin-related cerebellar dysplasia: definition of a distinct pattern of cerebellar malformation. *Eur Radiol.* 2017;27:5080–92.
58. Mencarelli A, et al. Epileptogenic brain malformations and mutations in tubulin genes: a case report and review of the literature. *Int J Mol Sci.* 2017;18:2273.
59. Fallet-Bianco C, et al. Neuropathological phenotype of a distinct form of lissencephaly associated with mutations in TUBA1A. *Brain.* 2008;131:2304–20.
60. Lecourtis M, et al. Human lissencephaly with cerebellar hypoplasia due to mutations in TUBA1A: expansion of the foetal neuropathological phenotype. *Acta Neuropathol.* 2010;119:779–89.
61. de Ligt J, et al. Diagnostic exome sequencing in persons with severe intellectual disability. *N Engl J Med.* 2012;367:1921–9.
62. Helbig KL, et al. Diagnostic exome sequencing provides a molecular diagnosis for a significant proportion of patients with epilepsy. *Genet Med.* 2016;18:898–905.
63. Lelieveld SH, et al. Meta-analysis of 2,104 trios provides support for 10 new genes for intellectual disability. *Nat Neurosci.* 2016;19:1194–6.
64. Posey JE, et al. Molecular diagnostic experience of whole-exome sequencing in adult patients. *Genet Med.* 2016;18:678–85.
65. Alby C, et al. Clinical, genetic and neuropathological findings in a series of 138 fetuses with a corpus callosum malformation. *Birth Defects Res A Clin Mol Teratol.* 2016;106:36–46.
66. Wisniewski W, et al. Comprehensive genomic analysis of patients with disorders of cerebral cortical development. *Eur J Hum Genet.* 2018;26:1121–31.
67. Sato T, et al. A case of tubulinopathy presenting with porencephaly caused by a novel missense mutation in the TUBA1A gene. *Brain and Development.* 2018;40:819–23.
68. Nogales E, Wolf SG, Downing KH. Structure of the alpha beta tubulin dimer by electron crystallography. *Nature.* 1998;391:199–203.
69. Amrom D, et al. Polymicrogyria with dysmorphic basal ganglia? Think tubulin! *Clin Genet.* 2014;85:178–83.
70. Maday S, Twelvetrees AE, Moughamian AJ, Holzbaur EL. Axonal transport: cargo-specific mechanisms of motility and regulation. *Neuron.* 2014;84:292–309.
71. Kerjan G, Gleeson JG. Genetic mechanisms underlying abnormal neuronal migration in classical lissencephaly. *Trends Genet.* 2007;23:623–30.
72. Fokkema IF, et al. LOVD v.2.0: the next generation in gene variant databases. *Hum Mutat.* 2011;32:557–63.
73. Kikkawa M, Hirokawa N. High-resolution cryo-EM maps show the nucleotide binding pocket of KIF1A in open and closed conformations. *EMBO J.* 2006; 25:4187–94.
74. Kellogg EH, et al. Near-atomic model of microtubule-tau interactions. *Science.* 2018;360:1242–6.

Ready to submit your research? Choose BMC and benefit from:

- fast, convenient online submission
- thorough peer review by experienced researchers in your field
- rapid publication on acceptance
- support for research data, including large and complex data types
- gold Open Access which fosters wider collaboration and increased citations
- maximum visibility for your research: over 100M website views per year

At BMC, research is always in progress.

Learn more biomedcentral.com/submissions

